PAPER

Check for updates

Microwave growth and tunable photoluminescence of nitrogen-doped graphene and carbon nitride quantum dots†

Siyong Gu, [iD] [a] Chien-Te Hsieh, [iD] ★[bc] Yasser Ashraf Gandomi, [iD] [ci] Jeng-Kuei Chang, [iD] ★[de] Ju Li, [iD] [d] Jianlin Li, [iD] [f] Houan Zhang,[a] Qing Guo, [iD] [gh] Kah Chun Lau[h] and Ravindra Pandey [iD] [g]

Tunable photoluminescent nitrogen-doped graphene and graphitic carbon nitride (g-C$_3$N$_4$) quantum dots are synthesized *via* a facile solid-phase microwave-assisted (SPMA) technique utilizing the pyrolysis of citric acid and urea precursors. The atomic ratio, surface functionalization, and atomic structure of as-prepared quantum dots strongly depend on the ratio of citric acid to urea. The quantum dots have a homogeneous particle size and tend to form a circle and/or ellipse shape to minimize the edge free energy. The atomic ratio of surface nitrogen to carbon (N/C) in the quantum dots can reach as high as 1.74, among the highest values reported in the literature. The SPMA technique is capable of producing high-quality quantum dots with photoluminescence (PL) emission at various wavelengths on a pilot scale. The atomic structures of the N-doped graphene and g-C$_3$N$_4$ quantum dots are explored using molecular dynamics simulations. Increasing the urea concentration increases the tendency of in-plane N (*i.e.*, quaternary N) substitution over that of other amino functionalizations, such as pyrrolic and pyridinic N. The PL emission can be precisely tuned *via* a one-step SPMA method by adjusting the precursor composition. A high quantum yield of 38.7% is achieved with N-doped graphene quantum dots, indicating the substantial influence of the N- and O-rich edge groups on the enhancement of PL efficiency. A bandgap structure is proposed to describe the interstate ($\pi^{\star}-\pi$) transition of quantum dots. This work introduces a novel approach for engineering the chemical composition and atomic structure of graphene and g-C$_3$N$_4$ quantum dots, facilitating their research and applications in optical, electronic, and biomedical devices.

[a] *Fujian Provincial Key Laboratory of Functional Materials and Applications, School of Materials Science and Engineering, Xiamen University of Technology, Xiamen 361024, P. R. China*

[b] *Department of Chemical Engineering and Materials Science, Yuan Ze University, Taoyuan 32003, Taiwan. E-mail: cthsieh@saturn.yzu.edu.tw*

[c] *Department of Mechanical, Aerospace, and Biomedical Engineering, University of Tennessee, Knoxville, TN 37996, USA*

[d] *Department of Nuclear Science and Engineering and Department of Materials Science and Engineering, Massachusetts Institute of Technology, Cambridge, MA 02139, USA*

[e] *Department of Materials Science and Engineering, National Chiao Tung University, Hsinchu 30010, Taiwan. E-mail: jkchang@nctu.edu.tw*

[f] *Energy and Transportation Science Division, Oak Ridge National Laboratory, TN 37831, USA*

[g] *Department of Physics, Michigan Technological University, Houghton, MI 49931, USA*

[h] *Department of Physics and Astronomy, California State University, Northridge, CA 91330, USA*

[i] *Department of Chemical Engineering, Massachusetts Institute of Technology, Cambridge, MA, USA*

† Electronic supplementary information (ESI) available. See DOI: 10.1039/c9tc00233b

Introduction

Photoluminescent carbon nanodots (CNDs) have attracted a lot of attention due to their environmental friendliness, green synthesis, and superior biocompatibility for biomedical applications compared to that of fluorescent semiconductor quantum dots, which are typically composed of toxic heavy metals (*e.g.*, Cd) to achieve high-intensity fluorescence.[1,2] CNDs, discovered in 2004, were initially prepared by purifying single-walled carbon nanotubes *via* an electrophoresis method.[3] CNDs (usually with an average size of below 10 nm) are a new class of carbon nanomaterials that shows great potential for a variety of applications including light-emitting diodes,[4] optical detectors,[5] bio-imaging probes,[6] and visible-light-driven photocatalysts.[7] Although carbon is a black conductive element, carbon-based quantum dots usually have semiconductor characteristics and strong luminescence, and are thus commonly referred to as carbon nano-lights.[8]

An ideal two-dimensional (2D) graphene sheet consists of sp^2-hybridized carbon atoms and is a zero-bandgap semiconductor.[9,10] One strategy for tuning the bandgap of graphene sheets is to reduce

the particle size down to <10 nm. This reduction in particle size alters the band structure due to quantum confinement and edge effects.[11,12] It has been demonstrated that photoluminescence (PL) properties can be tuned by controlling the size of graphene quantum dots (GQDs);[13,14] the PL emission exhibits a red-shift with increasing particle size. Theoretical calculations show that the highest occupied molecular orbital and the lowest unoccupied molecular orbital depend on the GQD size. Electron acceptor/donor addition can also be used to tailor the optical and electronic properties of graphene.

Recent progress in doping graphene with heteroatoms such as electron-rich nitrogen has enabled in-plane substitution of N atoms, making graphene an n-type semiconductor.[9,15] Several techniques have been utilized for synthesizing N-doped GQDs or CNDs, including a hydrothermal route using NH_4OH as the source of nitrogen,[9] chemical vapor deposition with pyridine as the source of both C and N,[15] pyrolysis of citric acid and ethanolamine precursors,[16] and pyrolysis of core–shell nanoparticles followed by dialysis.[17] N-doping, or amino functionalization, significantly alters the optical properties and PL intensity of GQDs.

Although some progress has been made in the synthesis of N-doped GQDs, challenges including the control of the N/C atomic ratio, group distribution, and bonding configuration still need to be overcome. N/C atomic ratios in the range of 5–15%, which lead to the formation of pyridinic or pyrrolic groups, have been reported.[9] N substitution is preferred over N decoration because it can be used to tailor the band structure and create novel atomic configurations (e.g., graphitic carbon nitride, g-C_3N_4 (g-CN))[18,19] if the appropriate N/C ratio is used. Pioneering studies have reported that g-CN powders were successfully synthesized by thermal poly-condensation of cyanamide at 400–600 °C[20] and pyrolysis of urea at 400–550 °C.[21] Recent efforts have been devoted to synthesizing g-CN nanoparticles at a moderate temperature, e.g., microwave mediated method from formamide at 180 °C for 0.5 h,[18] microwave-assisted solvothermal method of citric acid monohydrate, urea and oleic acid at 180 °C for 5 min under 4.6 bar,[19] and microwave-induced decomposition of an aqueous solution of citric acid and urea in a standard household microwave oven with a power of 700 W.[22] The achievements have demonstrated the other pathway to synthesize g-CN quantum dots under microwave irradiation. The development of techniques for synthesizing N-doped GQDs and g-CN quantum dots is thus important.

The present work develops an efficient and facile synthesis method for producing N-doped GQDs and g-CN quantum dots. The solid-phase microwave-assisted (SPMA) pyrolysis of citric acid with urea is used for the synthesis. The proposed method is suitable for large-scale production and enables precise control of the dopant concentration and thus the bonding structure of N-doped GQDs and g-CN quantum dots, leading to tunable PL emission and semiconducting properties.

Results and discussion

High-resolution transmission electron microscope (HR-TEM) micrographs of the CNDs prepared using solid-phase microwave-assisted (SPMA) pyrolysis are shown in Fig. 1(a)–(f). A homogeneous
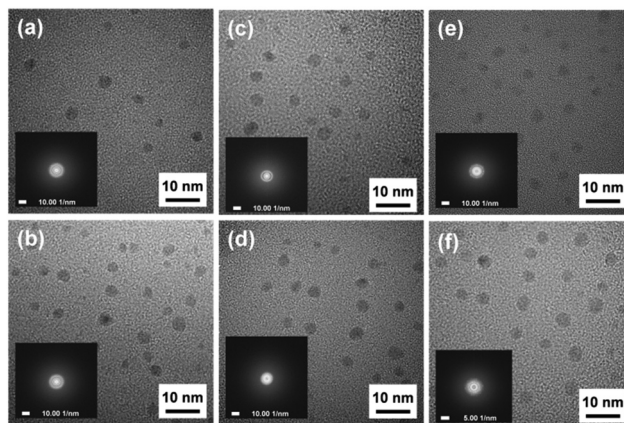

Fig. 1 HR-TEM micrographs of N-doped CND samples prepared using the SPMA method with C/U weight ratios of (a) 3/1, (b) 2/1, (c) 1/1, (d) 1/1.5, (e) 1/2, and (f) 1/3. Inset show the corresponding selected-area diffraction.

dispersion can be seen. The corresponding selected-area diffraction patterns, shown in the insets, indicate the presence of bright diffraction spots along with diffraction rings. The appearance of such bright rings suggests that the CNDs consisted of nano-crystallites. The particle size distribution of the as-prepared CNDs varies slightly with C/U weight ratio, as shown in the ESI† (see Fig. S1). The average particle sizes follow the order: 5.5 nm (C/U ratio: 3/1) > 4.6 nm (C/U ratio: 2/1) > 4.2 nm (C/U ratio: 1/1) > 3.5 nm (C/U ratio: 1/1.5) ≈ 3.5 nm (C/U ratio: 1/2) ≈ 3.5 nm (C/U ratio: 1/3). The morphology of CND samples was investigated by field-emission scanning electron microscopy (SEM). Top-view SEM images of the GQDs are given in Fig. S2 (ESI†), showing a large amount of nanoparticles dispersed over the carbon tape.

X-ray photon spectroscopy (XPS) was performed to investigate the chemical composition of N-doped CNDs. Fig. 2 shows a survey scan and C 1s and N 1s spectra of N-doped CNDs for C/U ratios of 3/1 and 1/3. In the XPS survey spectrum, the peak intensity of N 1s increases with decreasing C/U ratio. This indicates that the amount of urea determines the nitrogen
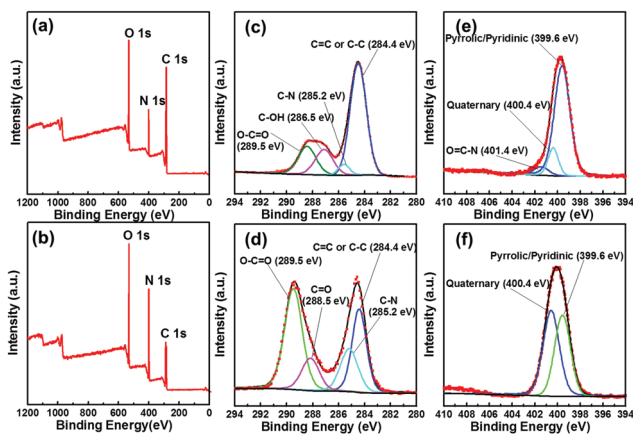

Fig. 2 XPS survey scan, C 1s, and N 1s spectra of N-doped CND samples for C/U ratios of (a, c and e) 3/1 and (b, d and f) 1/3.

This journal is © The Royal Society of Chemistry 2019

J. Mater. Chem. C, 2019, 7, 5468–5476 | 5469

concentration in CNDs. The C 1s spectra can be deconvoluted into five peaks centered at 284.4 eV (C=C or C–C), 285.2 eV (C–N), 286.5 eV (C–OH), 288.5 eV (C=O), and 289.5 eV (O–C=O), respectively, indicating various types of C-bonding.

Of note, the intensity of the C–N peak increases with decreasing C/U weight ratio. In a high-resolution scan of Fig. 2(e), an asymmetric N 1s peak can be precisely deconvoluted into signals for predominant pyrrolic and pyridinic N appearing at 399.6 eV, quaternary N at 400.4 eV, and N-oxides (e.g., O=C–N) at 401.4 eV.[9,15,18] The first peak is usually assigned to the presence of (sp^2) C–N=C (sp^2), in which nitrogen is bonded to two carbon atoms or a pyridine moiety, and the second peak refers to quaternary N, which is bonded to three sp^2 carbon atoms, known as graphitic nitrogen.[23,24] Graphitic nitrogen can refer to nitrogen atoms replacing carbon ones in a graphene lattice, in which the substitution maintains the sp^2 hybridization of C atoms, improving the electro-conductivity in graphene by donating delocalized electrons.[25–27] In contrast, both the pyridinic and quaternary N atoms are major contributors to the N 1s peak in Fig. 2(f); the ratio of pyridinic to quaternary N is significantly altered by the C/U weight ratio. Finally, the third peak is mainly attributed to the amide–carbonyl group (O=C–NH$_2$), e.g., amino and amide carbonyl functionalization at the edges of graphene sheets.[28,29]

To elucidate the atomic structure, the atomic ratios (including C, N, and O) are plotted versus C/U weight ratio in Fig. 3(a). As expected, both N- and O-rich CNDs can be synthesized at a low C/U weight ratio (e.g., C/U ratio of 1/2 or 1/3), while the C content remains relatively unchanged (about 55 at%) for C/U weight ratios of 1/1 and above. This reveals that a large amount of N doping (e.g., pyridinic and quaternary N) and O decoration (e.g., carboxylic, carbonyl, and phenolic groups) is present within the CND synthesized with a low C/U ratio.

Both N/C and O/C atomic ratios demonstrate a decreasing trend with increasing C/U weight ratio, as shown in Fig. 3(b).

At a C/U weight ratio of 1/2, an extremely high N/C ratio (174 at%) is achieved in the CND structure, which is much higher than reported values in the literature (e.g., 12.8 at% for the hydrothermal route in the presence of NH$_4$OH[9] and 58.4 at% for the microwave-assisted solvothermal method).[19] To the best knowledge of the authors, this is the highest N/C ratio within N-doped GQDs ever reported. This finding allows the development of tunable atomic structures, from N-doped GQD (mainly pyrrolic and pyridinic N) to g-CN, by controlling the chemical composition of the precursor (i.e., C/U weight ratio). An inductively-coupled plasma optical emission spectroscopy/mass spectrometry (ICP-OES/MS) was adopted to analyze the chemical compositions of all samples. The N/C atomic ratios show an order as 29.0% (C/U: 3/1) < 33.7% (C/U: 2/1) < 47.8% (C/U: 1/1) > 60.1% (C/U: 1/1.5) > 65.9% (C/U: 1/2) > 79.3% (C/U: 1/3), based on the analysis provided by the ICP-OES/MS. Thus, it can be deduced that the decreasing trend of N/C ratio follows the increasing trend of the of carbon source (i.e., citric acid) concentration within the precursor.

The deconvolution of the N 1s peak reveals further details regarding the structural composition. Fig. 3(c) shows the peak area ratios of substitutional N and pyrrolic or pyridinic N as a function of C/U weight ratio. As shown, quaternary N becomes more evident at low C/U weight ratios (i.e., 1/2–1/3). The ratio of pyridinic N to quaternary N is approximately 1.4, which is similar to that of triazine-based g-CN.[18] As shown in Fig. 3(d), the g-CN quantum dots formed at C/U weight ratios of 1/2–1/3. However, the elemental compositions obtained from XPS analysis are C$_3$N$_{5.2}$O$_{3.2}$ and C$_3$N$_{4.7}$O$_3$ for C/U ratios of 1/2 and 1/3, respectively. This discrepancy may be due to two reasons: (i) the XPS analysis only detects the surface chemical composition within a skin layer and (ii) the presence of oxygen is probably due to oxygen-containing functional groups at the edge of graphene sheets.[18] Based on the XPS analyses, the SPMA method is capable of producing N-doped GQDs (C/U ratio of 3/1–1/1.5) and/or g-CN quantum dots (C/U ratio of 1/2–1/3), depending on the precursor composition.

XRD was adopted to characterize the crystalline structure of CND samples. The XRD patterns are shown in Fig. 4(a). The intensity of the d_{002} main peak notably increases with decreasing C/U weight ratio, revealing enhanced crystallinity in the presence of urea during the SPMA process. Interestingly, the g-CN quantum dots prepared
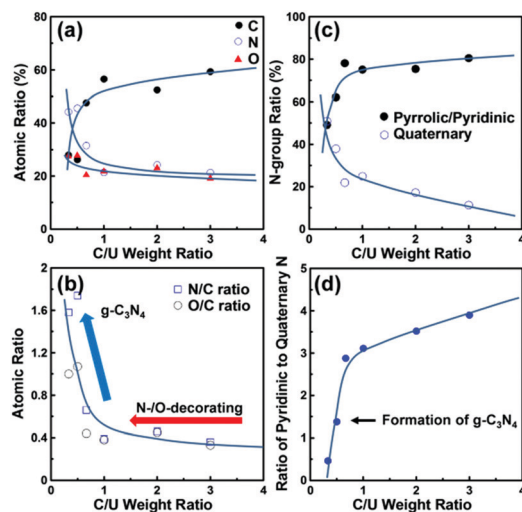

Fig. 3 (a) Various atomic ratios (including C, N, and O at%), (b) N/C and O/C atomic ratios, (c) molar ratio of N-functional group, and (d) molar ratio of pyridinic N to quaternary N as a function of C/U weight ratio.
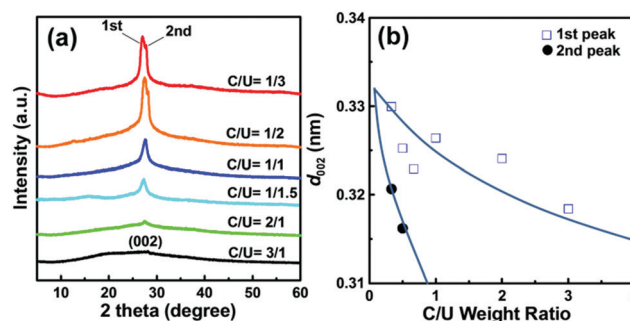

Fig. 4 (a) Typical XRD patterns of all CND samples and (b) corresponding interlayer spacing distances as a function of C/U weight ratio.

with C/U ratios of 1/2 and 1/3 exhibit twin peaks at *ca.* 27.0° (first peak) and *ca.* 28.0° (second peak), revealing two distinct types of layered structure within the g-CN crystalline configuration. Using Bragg's law, the d_{002} values are calculated to be 0.330 and 0.320 nm for the first and second peaks, respectively. The interlayer spacing distance determined from Bragg's law as a function of the C/U weight ratio is shown in Fig. 4(b). It is important to note that the interlayer distance (d_{002}) of perfect graphite is approximately 0.335–0.340 nm,[30] which is larger than that of all N-doped GQD and g-CN samples. This mainly originates from the N dopant in the layered graphite structure reducing the interlayer spacing distance since an N atom is smaller than a C atom. As expected, the d_{002} value for the first peak has a slightly decreasing trend with C/U weight ratio, whereas the second peak only appears at low C/U ratios. The presence of the second peak is most probably due to (i) the formation of g-CN crystals in the CNDs or (ii) N-induced shrinkage within the graphene sheets due to the presence of amino functionalities (*e.g.*, O and N decorations or N doping at the edge of g-CN quantum dots) or other structural defects.

To further evaluate the structure of the CNDs, Raman spectra were obtained using a laser beam at an excitation wavelength of 1048 nm. A typical Raman spectrum of the CND samples is provided in the ESI† (Fig. S3). Three main peaks are identified in the Raman spectra: the D band (1350 cm^{-1}), the G band (1580 cm^{-1}), and the 2D band (2700 cm^{-1}). The Raman band observed at 1580 cm^{-1} is ascribed to a single crystallite of graphite (G band). The D band at 1350 cm^{-1} is commonly attributed to amorphous carbon or deformation vibrations of a hexagonal ring.[31–33] The intensity ratio of D to G bands (I_D/I_G) can be considered as an indicator of the graphitic degree of carbon-based materials. As shown, the I_D/I_G ratios range from 0.94 to 0.97. This result reveals (i) that the CND samples obtained using the SPMA route have good crystallinity and (ii) that the influence of the C/U weight ratio on the crystallinity is minor. This trend could possibly result from several factors, including the existence of N and O decorations or N doping, the vibration of carbon atoms with dangling bonds within the crystal lattice plane, terminations of disordered graphite, and the defects in curved graphene sheets.[34] The position and shape of the 2D peak can be used to determine the number of graphene layers. The number of graphene layers was estimated to be in the range of 6–10 based on the standard Raman spectra at 514 nm.[35] However, it should be noted that the g-CN quantum dots may not obey the standard spectra due to the formation of a g-CN crystal structure in the samples prepared with low C/U weight ratios.

A schematic diagram describing the formation of various 2D atomic structures through the SPMA route is shown in Fig. 5. The 2D atomic structures have a tunable transition from N-doped GQDs to g-CN quantum dots controlled by the C/U weight ratio. The proposed atomic structures are based on the results of XPS analysis and the MD simulations. The SPMA process of growing N-doped GQDs consists of (i) the pyrolysis of citric acid (melting point: 156 °C) and urea (melting point: 135 °C), (ii) vapor-phase growth, and (iii) *in situ* N doping. Under microwave irradiation, the microwave energy is absorbed by the reactant and heating medium; thus, uniform and rapid heating is achieved.[36] Near the decomposition temperature, the pyrolysis of the carbon precursor
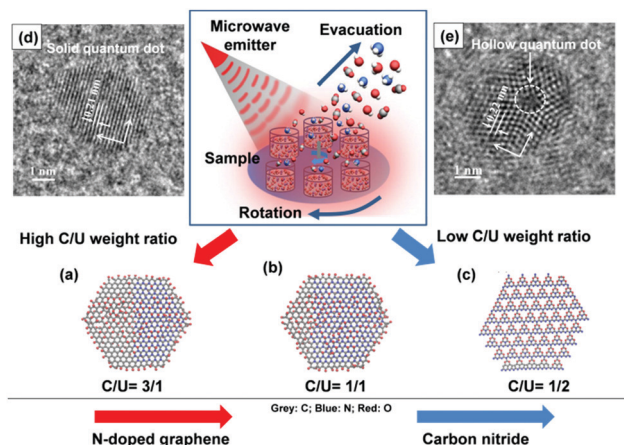

Fig. 5 Schematic diagram of 2D atomic structures created during SPMA process with C/U weight ratios of (a) 3/1, (b) 1/1, and (c) 1/2, simulated by the MD software. HR-TEM micrographs for the CNDs prepared with C/U ratios of (e) 3/1 and (f) 1/2.

produces a large amount of free radicals, such as methyl (CH$_3$•), hydroxyl (OH•) and amino (NH$_2$•) radicals, for the vapor-phase growth of CNDs. Meanwhile, *in situ* N and O decoration and N doping take place, forming sp^2-hybridized C–N and C–O bonds within the as-grown CND structure during a relatively short time frame (5 min in this case). Microwave heating not only reduces the total time required for the chemical reaction by several orders of magnitude, but also suppresses side reactions and thus facilitates the yield and reproducibility of a specific synthesis protocol.[37,38]

To confirm the existence of the proposed atomic structures at ambient temperature, molecular dynamics (MD) simulations were conducted to verify four atomic configurations produced from the chemical precursor (C/U ratio of 1/2) during the SPMA process. The models are shown in Fig. S4 (ESI†). The MD simulations were performed using LAMMPS with the Reax force field.[39–41] Two kinds of atomic structure were considered: (i) heavily N-doped graphene with O adsorption and (ii) heavily O-doped g-CN. For case (i), it is inferred that O atoms are likely to adsorb on the edge C sites and form C=O bonds (model 1), as shown in Fig. S4(a) (ESI†). Although in C/N binary models C atoms preferentially concentrate in the center, fewer edge C=O bonds can be formed when O atoms are added. Fig. S4(b) (ESI†) shows the model built for C atoms gathering at the edge of the flake and forming more C=O bonds (model 2) compared to those in model 1. This model has lower total energy, indicating that edge C atoms are more favourable than inner C atoms because of the higher C=O formation rate. Of note, in this model, armchair edges with a C=O bond are not stable. Thus, a hexagonal model with zigzag edges was built (model 3), where the O atoms saturate the outermost C atoms, as shown in Fig. S4(c) (ESI†). With the lowest total energy, model 3 indicates that C=O bonds are likely to be formed at the zigzag edge of N-doped graphene models. Several hole defects were manually created in model 3. The increased total energy suggests that sparse or random defects are unfavorable. A comparison of total energy is given in Table S1 (ESI†).

For case (ii), the only way to get a g-CN-based flake while maintaining the C–N–O ratio is to substitute some N atoms by O atoms.[42] A heavily O-doped g-CN flake (model 4) was created, as shown in Fig. S3(d) (ESI†). The thermal equilibration at approximately 227 °C (10 ps) suggests that the atomic configuration is stable. The total energy is $-108\,426$ kcal mol^{-1}, which is the lowest among these four models. This indicates that the O-doped g-CN flake is likely to be formed with a high N/C ratio, which is identical with previous study.[22] To confirm this, the N/C ratio in model 3 (Fig. S5(a, c), ESI†) and model 4 (Fig. S5(b, d), ESI†) was reduced and the total energies were compared; the results are listed in Table S2 (ESI†). When the N/C ratio is reduced, model 3 becomes more favorable, indicating that N-doped graphene structures preferentially form with a lower N/C ratio, which is in accordance with the experimental observations (XPS N peaks). These simulation results suggest that: (i) the most favorable O adsorption sites in N-doped graphene are the edge sites of carbon and (ii) O-adsorbed N-doped graphene flakes are prone to form in samples with low N/C ratios, and O-doped g-CN-like structures preferentially form in samples with high N/C ratios.

The capability of reaching a CND yield that is suitable for industry is of great importance. The yield was determined from the weight loss after the SPMA process. The yield values were 48, 45, 42, 41, 40, and 38 wt% for samples with C/U ratios of 3/1, 2/1, 1/1, 1/1.5, 1/2, and 1/3, respectively. This indicates that citric acid improves the CND yield. The satisfactory yield indicates the feasibility of producing high-quality CNDs in a large scale when using a continuous operation of the microwave reactor.

It can be postulated that the substitutional N gradually replaces pyrrolic or pyridinic N during the pyrolysis processes at high N concentrations (i.e., low C/U ratios). Therefore, the atomic structure transforms from N-doped GQDs (i.e., pyrrolic and pyridine N) to g-CN quantum dots (i.e., quaternary N), as shown in Fig. 5(a)–(c). To further support this assertion, HR-TEM micrographs of the CNDs prepared with C/U ratios of 3/1 and 1/2 are shown in Fig. 5(d) and (e), respectively. Both CND single particles exhibit good crystallinity with a lattice distance of 0.21–0.22 nm, corresponding to the $(11\bar{2}0)$ lattice fringes of graphene sheets.[43] However, the former possesses a layered crystal structure, while the latter one consists of several triangular domains, forming a circular shape. This observation is consistent with the proposed atomic structures. The circular sharpness (Φ) of an individual CND is defined by the ratio of the lateral length perpendicular to the $\langle 11\bar{2}0 \rangle$ direction to that along the $\langle 11\bar{2}0 \rangle$ direction. The Φ values are determined to be 0.72 and 0.86 for C/U weight ratios of 2/1 and 1/2, respectively. This finding reveals that the former exhibits an elliptical shape, while the latter tends to exhibit a circular shape. Both configurations prefer to form circular peripheries in thermodynamic equilibrium structures to minimize edge free energies through atomic migration, rearrangement of atoms (e.g., C, N, O), and reconstruction of crystallization.[44,45]

Fig. 6(a) shows ultraviolet-visible (UV-vis) absorption spectra of the CND samples in distilled water. There is an absorption lump at ca. 330 nm and a broadened shoulder at ca. 410 nm.
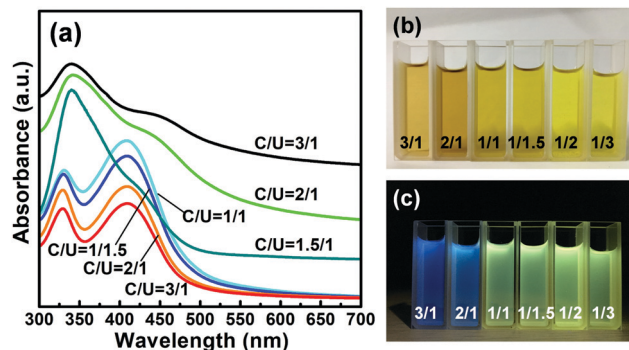

Fig. 6 (a) UV-vis absorption spectra of all CND samples in distilled water and photographs of each CND suspension under (b) visible light and (c) UV illumination at 360 nm.

The absorption band centered at 330 nm can be attributed to the typical absorption pattern of g-CN or n-type semiconductors.[19,46,47] The absorption band at 410 nm mainly originates from the surface molecular center[48] and its absorption edge is ascribed to the (n → π*) transitions of the nonbonding electrons of adatoms.[49–51] It can be deduced that the edge of the absorption band becomes more evident with decreasing C/U weight ratio. As expected, the surface density of adatoms or molecules adsorbed onto the quantum dots increases at low C/U ratios, thereby altering the surface state of CNDs, i.e., the intermediate states within the (π → π*) region. Fig. 6(b) and (c) show photographs of each CND suspension under visible light and UV illumination at 360 nm, respectively. Clearly, the CND samples emit different emission colors: deep blue, blue, deep green, green, green, yellow, and yellow (i.e., a red-shift behavior) under UV illumination. Due to their similar particle size distributions, this result indicates that the PL emission characteristics of the quantum dots are strongly affected by the chemical composition and atomic structure.

The PL emission spectra of CND suspensions with C/U weight ratios of 3/1 and 1/3 excited at various wavelengths are shown in Fig. 7(a) and (b), respectively. The CND suspensions exhibit tunable PL emission, which is mainly controlled by the C/U weight ratio in the SPMA process. As shown in Fig. 7(a), the N-doped GQDs prepared with a C/U ratio of 3/1 display an asymmetric peak ranging from 400 to 525 nm under 380 nm excitation. The strongest PL appears at ca. 430 nm (2.88 eV). In contrast, as shown in Fig. 7(b), the g-CN quantum dots prepared with a C/U ratio of 1/3 show a twin PL peak under 380 nm excitation, at ca. 450 nm (2.76 eV) and 512 nm (2.42 eV), revealing a red shift due to the O and N doping and the formation of g-CN crystals. Both CND suspensions exhibit a major PL peak under excitation by visible light (450 nm), concentrated at 525–530 nm (2.34–2.36 eV). Therefore, it can be inferred that the quantum dots display excitation-dependent PL emission. Since the CND suspensions still exhibit visible PL emission under visible-light illumination, this is presumably due to the minimization of thermal loss or the formation of an excited-state relaxation channel.[52]

To explore the tunable PL behavior, a single-bandgap structure for describing the (π*–π) transition of CND samples is proposed,

5472 | J. Mater. Chem. C, 2019, 7, 5468–5476

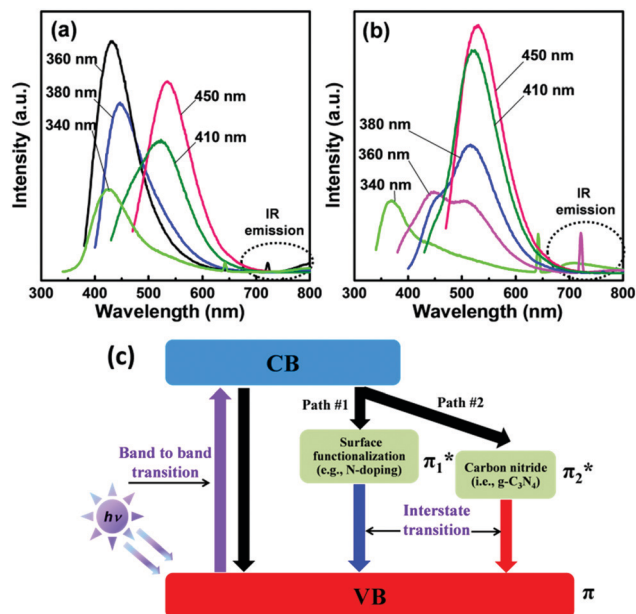This journal is © The Royal Society of Chemistry 2019

Fig. 7 PL emission spectra of various CND suspensions prepared using SPMA route with C/U ratios of (a) 3/1 and (b) 1/3, excited at different wavelengths. (c) Band-gap structure describing the ($\pi^*-\pi$) transition of CND samples, where CB and VB represent conduction and valence bands, respectively.

as illustrated in Fig. 7(c). This tunable PL is based on the zigzag effect caused by band-to-band and interstate transitions. The presence of chemical doping (*e.g.*, N dopant) in C=C sp^2 domains and amino-edge functional groups usually influences the bonding and anti-bonding molecular orbitals, leading to different electronic transition states.[29] On the surface of CNDs, some oxygenated moieties are replaced by amino functional groups, which serve as new radiative recombination sites.[53,54] The amino and oxygen functionalization levels are prone to narrowing the energy gap of ($\pi_1^*-\pi$), thus allowing a pathway for crossing the interstate transition, *i.e.*, path #1. Path #2 provides another route for PL emission in the presence of g-CN crystals in the CND samples, creating the other energy gap of ($\pi_2^*-\pi$). The g-CN quantum dots (prepared with a C/U ratio of 1/2 to 1/3) have a high level of g-CN crystallization and high N or O functionalization extent at the edges, inducing the coexistence of both path #1 and #2. This description can be used to explain why the g-CN quantum dots have twin PL emissions excited at 360 nm. Besides the only PL peak excited at 450 nm, all CND samples tend to be partially excited by the blue light, thus obeying path #1 due to the presence of the edge functionalization or surface defects.[19] Based on this, the wavelength-dependent PL modulation tuned by the C/U weight ratio is consistent with the proposed bandgap structure.

The quantum yield (Θ) values of the samples were calculated. They follow the order 36.7% (C/U: 3/1) > 31.4% (C/U: 2/1) > 29.0% (C/U: 1/1) > 28.1% (C/U: 1/1.5) > 26.7% (C/U: 1/2) > 26.3% (C/U: 1/3). It has reported that g-CN quantum dots show strong blue fluorescence with fluorescence quantum yield of 29.0%, whereas the highest reported quantum yield of graphene

dots is 11.4%.[55] The quantum yield of our sample is vastly higher compared to the other GQDs reported elsewhere (*i.e.*, from 2 to 22.9%).[56,57] This sequence is analogous to the increasing trend of quaternary N ratio in the CND samples. The highly efficient PL emission mainly originates from high electron-withdrawing possibility.[9] The N- and O-rich edge groups are believed to be major contributors to the enhancement of PL efficiency. However, excessive N dopant content or amount of substitutional N atoms could induce PL quenching, which is attributed to deactivated zigzag-edge sites and ineffective energy transfer between the N dopant and the carbon surface.[58] This is the major reason that the N-doped GQDs prepared with a C/U ratio of 3/1 had the highest fluorescence intensity among all samples.

Interestingly, both CND samples exhibit near infrared (NIR) emission under UV irradiation at 360 nm, as shown in Fig. 7(a) and (b). However, the CND suspension prepared with a C/U ratio of 1/3 emits high-intensity NIR light, much stronger than that emitted by the sample with a C/U ratio of 3/1. The maximum NIR intensity of the CND suspensions is at approximately 720 nm. It has been reported that π-electrons and large macromolecular domains are related to the NIR PL mechanism observed in N-doped GQDs.[59] This NIR emission possibly originates from the presence of g-CN crystallites. This phenomenon indicates potential applications involving thermal management of electronic devices and fluorescence imaging *in vivo*.

Finally, the practical applicability and environmental friendliness of N-doped CNDs prepared using the SPMA method were examined. The as-prepared CND samples can be uniformly dispersed in water, and thus form well-dispersed suspensions. There were almost no sediments in the CND suspensions after several months, as shown in Fig. S6 (ESI†). To sum up, the SPMA approach offers a facile and effective route for finely tuning the PL emission of quantum dots, resulting from changes in various properties, such as chemical composition, atomic structure, band-gap structure, and surface functionalization level.

Conclusions

The SPMA method was applied to synthesize N-doped GQDs and g-CN quantum dots using the pyrolysis of citric acid and urea during a one-pot synthesis process. A high yield and high production rate of as-prepared quantum dots were reached on a pilot scale. The facile SPMA fabrication of N-doped GQDs and g-CN quantum dots allows controllable chemical composition, atomic structure, and tunable PL emission. The quantum dots were found to have a narrow particle size distribution and a circular or elliptical shape to minimize the edge free energy. XPS analysis showed that the in-plane N substitution (*i.e.*, quaternary N) was preferred when using high concentration of urea. The N/C atomic ratio in the quantum dots reached as high as 174%, which is much higher than values reported in the literature. MD simulations were conducted to explore the atomic structures of N-doped graphene and g-CN quantum dots prepared using the one-step SPMA method. The tunable PL emission could be precisely controlled by the N concentration and atomic

structure of quantum dots. The N-doped GQDs exhibited the highest quantum yield (38.7%) among the CND samples, revealing that the N- and O-rich edge groups are major contributors to the enhancement of PL efficiency. A bandgap structure was proposed for describing the interstate (π^*–π) transition of quantum dots. This work proposed an efficient SPMA approach for synthesizing graphene and g-CN quantum dots with controllable chemical composition and atomic structure, allowing for potential applications, particularly in optical, semiconductor, and biological devices.

Experimental section

Synthesis of N-doped GQDs and g-CN quantum dots

As-received citric acid (Sinopharm Chemical Reagent Co., analytical reagent), urea (Sinopharm Chemical Reagent Co., analytical reagent), sulfuric acid (Sinopharm Chemical Reagent Co., analytical reagent), sodium hydroxide (Sinopharm Chemical Reagent Co., analytical reagent), and ultrapure water, prepared with a Milli-Q system (Millipore, Bedford, MA, USA), were used for the synthesis. N-doped GQDs and g-CN quantum dots were synthesized *via* an SPMA method using a mixture of citric acid and urea as the precursor with six citric acid/urea (C/U) weight ratios (3/1, 2/1, 1/1, 1/1.5, 1/2, and 1/3). A three-dimensional ball mixer was utilized to uniformly mix the citric acid and urea. The precursor (100 g) was placed in a 500 mL quartz tube, into which 10 mL of distilled water was added. The SPMA reactor was equipped with a microwave emitter (with a nominal power of 6000 W) and a rotary reaction base (with a maximum rotation speed of 60 rpm). The reactor could accommodate six reaction tubes (diameter: 150 mm; height: 60 mm) simultaneously under microwave irradiation.

For sample preparation, the precursor was heated at 250 °C for 5 min with a rotation speed of 60 rpm while the internal pressure was maintained at ambient pressure during the microwave-assisted synthesis process. Immediately after the SPMA reaction, brown and black CNDs were obtained. The CNDs were ball-milled and then sieved through a metallic screen (#200 mesh). The solid product was dispersed and washed using ultrapure water, and finally centrifuged at 15 000 rpm for 0.5 h.

Characterization of N-doped GQDs and g-CN quantum dots

The morphologies of the N-doped GQD and g-CN quantum dot samples were investigated *via* SEM (Zeiss ULTRA 55, Jena) and HR-TEM (FEI Talos F200s). An X-ray diffractometer (Shimadzu Labx XRD-6000), equipped with a Cu-Kα emitter, was used to characterize crystallinity. The bonding structure of GQD and g-CN samples was analyzed using Raman spectroscopy (Renishaw Micro-Raman spectrometer). The chemical composition of the samples was further examined using XPS (Fison VG ESCA210). The C 1s, N 1s, and O 1s spectra were deconvoluted using the non-linear least squares fitting algorithm with a symmetric Gaussian function.

An UV-vis spectrometer (Agilent Technology Cary 60) was employed to analyze the absorbance spectra of N-doped GDQ and g-CN suspensions. A scan rate of 60 nm min^{-1} was used,

and each suspension was prepared with a concentration of 200 mg powder/1000 mL distilled water within the quartz cells. A fluorescence spectrometer (Hitachi F-7000 FLS920P) was adopted to analyze the PL emission spectra. The PL measurements were carried out at wavelengths of 340, 366, 380, 410, and 450 nm. The Θ value was quantified with reference to Rhodamine B (Θ: 95% at 552 nm excitation) using the following equation:

$$\Theta = \Theta_{reference} \times [(PL\ area/OD)_{sample}/(PL\ area/OD)_{reference}]$$
$$\times \eta_{sample}^{2}/\eta_{reference}^{2}$$

where the subscripts "sample" and "reference" indicate the sample and standard quantum dots, respectively. η is the reflective index of the solvent, and PL area and OD are the fluorescence area and absorbance value, respectively.

Molecular dynamics simulations

MD simulations were performed to simulate the N doping and N decoration of 2D graphene sheets (*i.e.*, N-doped GQDs and g-CN atomic structures). MD simulations were carried out using the software package Large-scale Atomic/Molecular Massively Parallel Simulator (LAMMPS) with the Reax force field. An ICP-OES/MS was adopted to analyze the chemical compositions of the samples. The total number of atoms was 740 (structure size: 40–50 Å) and the C : N : O ratio was 325 : 215 : 200, which is in accordance with the ICP-OES/MS results for the sample with a C/U ratio of 1/2. The whole simulation ran with a canonical ensemble using the Nosé–Hoover thermostat at room temperature ($\sim$27 °C) for 10 ps with a time step of 0.1 fs. The simulation box size was 80 $\times$ 80 $\times$ 40 Å^3, and thus the separation between two neighboring images was larger than 35 Å in all three dimensions. This setup can effectively eliminate interactions between replicas.

Conflicts of interest

There are no conflicts to declare.

Acknowledgements

References

1 X. Zhai, P. Zhang, C. Liu, T. Bai, W. Li, L. Dai and W. Liu, *Chem. Commun.*, 2012, **48**, 7955.

2 S. K. Bhunia, A. Saha, A. R. Maity, S. C. Ray and N. R. Jana, *Sci. Rep.*, 2013, **3**, 1473.

3 X. Xu, R. Ray, Y. Gu, H. J. Ploehn, L. Gearheart, K. Raker and W. A. Scrivens, *J. Am. Chem. Soc.*, 2004, **126**, 12736.

4 X. Guo, C. Wang, Z. Yu, L. Chen and S. Chen, *Chem. Commun.*, 2012, **48**, 2692.

5 A. Zhu, Q. Qu, X. Shao, B. Kong and Y. Tian, *Angew. Chem., Int. Ed.*, 2012, **51**, 7185.

5474 | *J. Mater. Chem. C*, 2019, **7**, 5468–5476

This journal is © The Royal Society of Chemistry 2019

6 Q. Li, T. Y. Ohulchanskyy, R. Liu, K. Koynov, D. Wu, A. Best, R. Kumar, A. Bonoiu and P. N. Prasad, *J. Phys. Chem. C*, 2010, **114**, 12062.

7 B. Y. Yu and S. Kwak, *J. Mater. Chem.*, 2012, **22**, 8345.

8 S. N. Baker and G. A. Baker, *Angew. Chem., Int. Ed.*, 2010, **49**, 6726.

9 Y. Dai, H. Long, X. Wang, Y. Wang, Q. Gu, W. Jiang, Y. Wang, C. Li, T. H. Zeng, Y. Sun and J. Zeng, *Part. Part. Syst. Charact.*, 2014, **31**, 597.

10 D. Wei, Y. Liu, Y. Wang, H. Zhang, L. Huang and G. Yu, *Nano Lett.*, 2009, **9**, 1752.

11 L. Jiao, X. Wang, G. Diankov, H. Wang and H. Dai, *Nat. Nanotechnol.*, 2010, **5**, 321.

12 W. Liu, X. Yan, J. Chen, Y. Feng and Q. Xue, *Nanoscale*, 2013, **5**, 6053.

13 H. Li, X. He, Z. Kang, H. Huang, Y. Liu, J. Liu, S. Lian, C. H. A. Tsang, X. Yang and S. Lee, *Angew. Chem., Int. Ed.*, 2010, **49**, 4430.

14 Y. Wang and A. Hu, *J. Mater. Chem. C*, 2014, **2**, 6921.

15 Z. Jin, J. Yao, C. Kittrell and J. M. Tour, *ACS Nano*, 2011, **5**, 4112.

16 M. J. Krysmann, A. Kelarakis, P. Dallas and E. P. Giannelis, *J. Am. Chem. Soc.*, 2011, **134**, 747.

17 Y. Wang, L. Dong, R. Xiong and A. Hu, *J. Mater. Chem. C*, 2013, **1**, 7731.

18 S. Barman and M. Sadhukhan, *J. Mater. Chem.*, 2012, **22**, 21832.

19 X. Cao, J. Ma, Y. Lin, B. Yao, F. Li, W. Weng and X. Lin, *Spectrochim. Acta, Part A*, 2015, **151**, 875.

20 X. Wang, K. Maeda, A. Thomas, K. Takanabe, G. Xin, J. M. Carlsson, K. Domen and M. Antonietti, *Nat. Mater.*, 2009, **8**, 76.

21 J. Liu, T. Zhang, Z. Wang, G. Dawson and W. Chen, *J. Mater. Chem.*, 2011, **21**, 14398.

22 L. Sciortino, A. Sciortino, R. Popescu, R. Schneider, D. Gerthsen, S. Agnello, M. Cannas and F. Messina, *J. Phys. Chem. C*, 2018, **122**, 19897.

23 R. Arrigo, M. Hävecker, R. Schlögl and D. S. Su, *Chem. Commun.*, 2008, 4891.

24 Y. Shao, S. Zhang, M. H. Engelhard, G. Li, G. Shao, Y. Wang, J. Liu, I. A. Aksay and Y. Lin, *J. Mater. Chem.*, 2010, **20**, 7491.

25 A. L. Lherbier, X. Blase, Y. Niquet, F. O. Triozon and S. R. Roche, *Phys. Rev. Lett.*, 2008, **101**, 36808.

26 L. Yan, Y. B. Zheng, F. Zhao, S. Li, X. Gao, B. Xu, P. S. Weiss and Y. Zhao, *Chem. Soc. Rev.*, 2012, **41**, 97.

27 J. O. Hwang, J. S. Park, D. S. Choi, J. Y. Kim, S. H. Lee, K. E. Lee, Y. Kim, M. H. Song, S. Yoo and S. O. Kim, *ACS Nano*, 2011, **6**, 159.

28 H. Tetsuka, R. Asahi, A. Nagoya, K. Okamoto, I. Tajima, R. Ohta and A. Okamoto, *Adv. Mater.*, 2012, **24**, 5333.

29 K. Sandeep, G. R. Roy, D. Sen, U. K. Ghorai, R. Thapa, N. Mazumder, S. Saha and K. K. Chattopadhyay, *Nanoscale*, 2014, **6**, 3384.

30 C. Hsieh, C. Lin, Y. Chen, J. Lin and H. Teng, *Carbon*, 2013, **62**, 109.

31 Y. T. Lee, N. S. Kim, J. Park, J. B. Han, Y. S. Choi, H. Ryu and H. J. Lee, *Chem. Phys. Lett.*, 2003, **372**, 853.

32 K. Kim, K. Kim, W. S. Jung, S. Y. Bae, J. Park, J. Choi and J. Choo, *Chem. Phys. Lett.*, 2005, **401**, 459.

33 L. Ni, K. Kuroda, L. Zhou, T. Kizuka, K. Ohta, K. Matsuishi and J. Nakamura, *Carbon*, 2006, **44**, 2265.

34 C. Huang, C. Hsu, P. Kuo, C. Hsieh and H. Teng, *Carbon*, 2011, **49**, 895.

35 A. C. Ferrari, J. C. Meyer, V. Scardaci, C. Casiraghi, M. Lazzeri, F. Mauri, S. Piscanec, D. Jiang, K. S. Novoselov, S. Roth and A. K. Geim, *Chem. Phys. Lett.*, 2006, **97**, 187401.

36 G. Yang, Y. Kong, W. Hou and Q. Yan, *J. Phys. Chem. B*, 2005, **109**, 1371.

37 B. Idalia and N. Markus, *Nanoscale*, 2010, **2**, 1358.

38 F. Xu, G. Zhang, F. Zhang and Y. Zhang, *Appl. Surf. Sci.*, 2015, **349**, 437.

39 S. Plimpton, *J. Comput. Phys.*, 1995, **117**, 1.

40 T. R. Mattsson, J. M. D. Lane, K. R. Cochrane, M. P. Desjarlais, A. P. Thompson, F. Pierce and G. S. Grest, *Phys. Rev. B: Condens. Matter Mater. Phys.*, 2010, **81**, 054103.

41 H. M. Aktulga, J. C. Fogarty, S. A. Pandit and A. Y. Grama, *Parallel Comput.*, 2012, **38**, 245.

42 F. Wei, Y. Liu, H. Zhao, X. Ren, J. Liu, T. Hasan, L. Chen, Y. Li and B.-L. Su, *Nanoscale*, 2018, **10**, 4515.

43 J. Peng, W. Gao, B. K. Gupta, Z. Liu, R. Romero-Aburto, L. Ge, L. Song, L. B. Alemany, X. Zhan, G. Gao, S. A. Vithayathil, B. A. Kaipparettu, A. A. Marti, T. Hayashi, J. Zhu and P. M. Ajayan, *Nano Lett.*, 2012, **12**, 844.

44 T. Xu, K. Yin, X. Xie, L. He, B. Wang and L. Sun, *Small*, 2012, **8**, 3422.

45 X. Jia, M. Hofmann, V. Meunier, B. G. Sumpter, J. Campos-Delgado, J. M. Romo-Herrera, H. Son, Y. H. Hsieh, A. Reina, J. Kong, M. Terrones and M. S. Dresselhaus, *Science*, 2009, **323**, 1701.

46 A. Thomas, A. Fischer, F. Goettmann, M. Antonietti, J. Müller, R. Schlögl and J. M. Carlsson, *J. Mater. Chem.*, 2008, **18**, 4893.

47 J. Zhou, Y. Yang and C. Zhang, *Chem. Commun.*, 2013, **49**, 8605.

48 M. Xu, G. He, Z. Li, F. He, F. Gao, Y. Su, L. Zhang, Z. Yang and Y. Zhang, *Nanoscale*, 2014, **6**, 10307.

49 T. Yeh, W. Huang, C. Chung, I. Chiang, L. Chen, H. Chang, W. Su, C. Cheng, S. Chen and H. Teng, *J. Phys. Chem. Lett.*, 2016, **7**, 2087.

50 G. Eda, Y. Lin, C. Mattevi, H. Yamaguchi, H. Chen, I. Chen, C. Chen and M. Chhowalla, *Adv. Mater.*, 2010, **22**, 505.

51 F. Liu, M. Jang, H. D. Ha, J. Kim, Y. Cho and T. S. Seo, *Adv. Mater.*, 2013, **25**, 3657.

52 S. Kim, S. W. Hwang, M. Kim, D. Y. Shin, D. H. Shin, C. O. Kim, S. B. Yang, J. H. Park, E. Hwang, S. Choi, G. Ko, S. Sim, C. H. Sone, J. Choi, S. Bae and B. H. Hong, *ACS Nano*, 2012, **6**, 8203.

53 S. Zhu, J. Zhang, S. Tang, C. Qiao, L. Wang, H. Wang, X. Liu, B. Li, Y. Li, W. Yu, X. Wang, H. Sun and B. Yang, *Adv. Funct. Mater.*, 2012, **22**, 4732.

This journal is © The Royal Society of Chemistry 2019

J. Mater. Chem. C, 2019, **7**, 5468–5476 | **5475**

54 J. Shen, Y. Zhu, C. Chen, X. Yang and C. Li, *Chem. Commun.*, 2011, **47**, 2580.

55 S. Zhu, J. Zhang, C. Qiao, S. Tang, Y. Li, W. Yuan, B. Li, L. Tian, F. Liu, R. Hu, H. Gao, H. Wei, H. Zhang, H. Sun and B. Yang, *Chem. Commun.*, 2011, **47**, 6858.

56 Z. Zhang, J. Zhang, N. Chen and L. Qu, *Energy Environ. Sci.*, 2012, **5**, 8869.

57 L. Li, G. Wu, G. Yang, J. Peng, J. Zhao and J. J. Zhu, *Nanoscale*, 2013, **5**, 4015.

58 F. Schedin, A. K. Geim, S. V. Morozov, E. W. Hill, P. Blake, M. I. Katsnelson and K. S. Novoselov, *Nat. Mater.*, 2007, **6**, 652.

59 L. Tang, R. Ji, X. Li, G. Bai, C. P. Liu, J. Hao, J. Lin, H. Jiang, K. S. Teng, Z. Yang and S. P. Lau, *ACS Nano*, 2014, **8**, 6312.

Electronic Supporting Information

for

Microwave Growth and Tunable Photoluminescence of Nitrogen-doped

Graphene and Carbon Nitride Quantum Dots

Table S1.   Total energy comparison for Model 1-4.

Model No.	Configuration	Total energy (kcal/mole)
1	Figure S3(a)	-107,339
2	Figure S3(b)	-107,507
3	Figure S3(c)	-107,715
4	Figure S3(d)	-108,426

Table S2.   Total energy comparison with different N/C ratios.

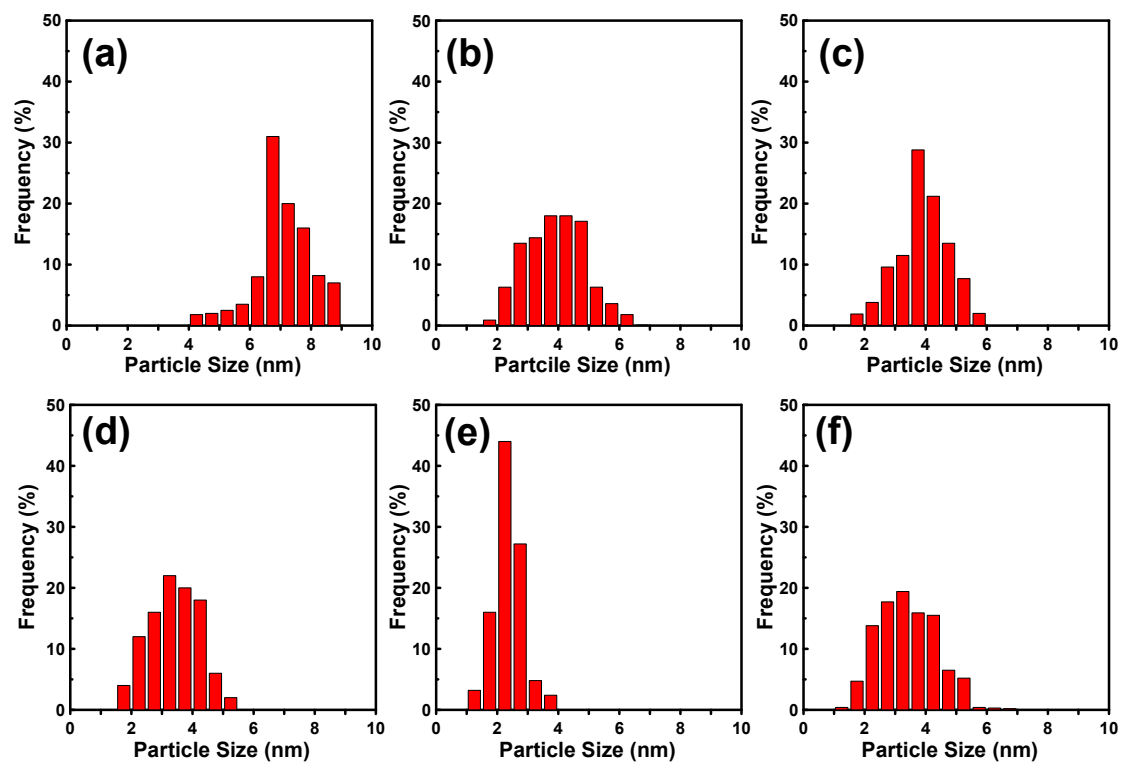| No.	C/U ratio	N/C atomic ratio	Configuration	Total energy (kcal/mol)
1	3/1	15/53	Figure S4(c)	**-115,470**
2			Figure S4(d)	-113,975
3	1/1	24/49	Figure S4(a)	**-110,556**
4			Figure S4(b)	-110,303
5	1/2	27/29	Figure S3 (c)	-107,715
6			Figure S3(d)	**-108,426**

Figure S1.　Particle size distributions of N-doped CND samples prepared using the SPMA method with C/U weight ratios of (a) 3/1, (b) 2/1, (c) 1/1, (d) 1/1.5, (e) 1/2, and (f) 1/3.
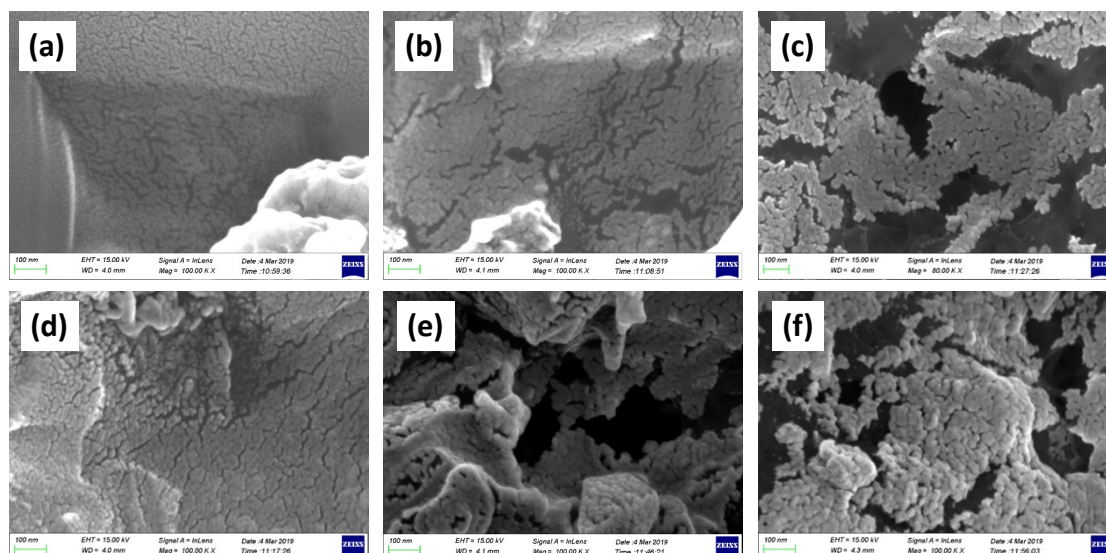
Figure S2.   SEM micrographs of N-doped CND samples prepared using the SPMA method with C/U weight ratios of (a) 3/1, (b) 2/1, (c) 1/1, (d) 1/1.5, (e) 1/2, and (f) 1/3.
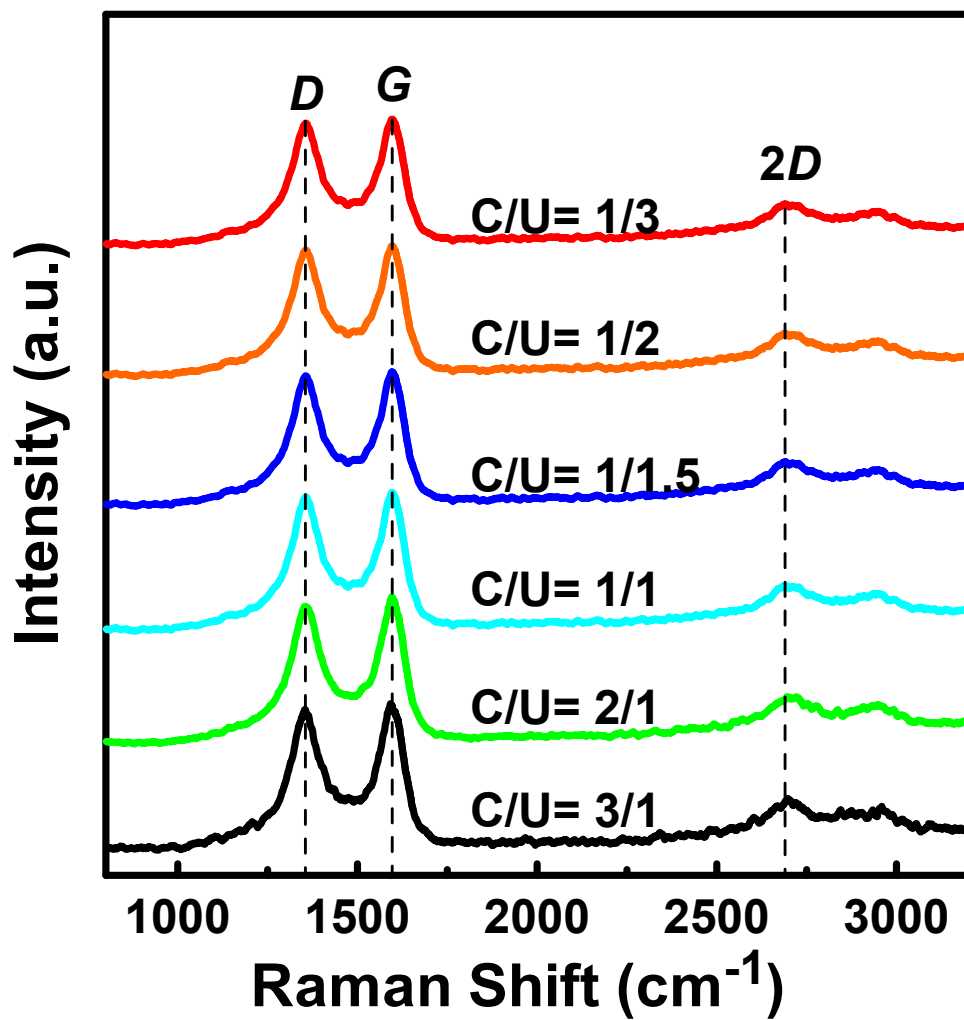
Figure S3. Typical Raman spectra of CND samples determined by the laser at 514 nm excitation wavelength.

(a)

(b)

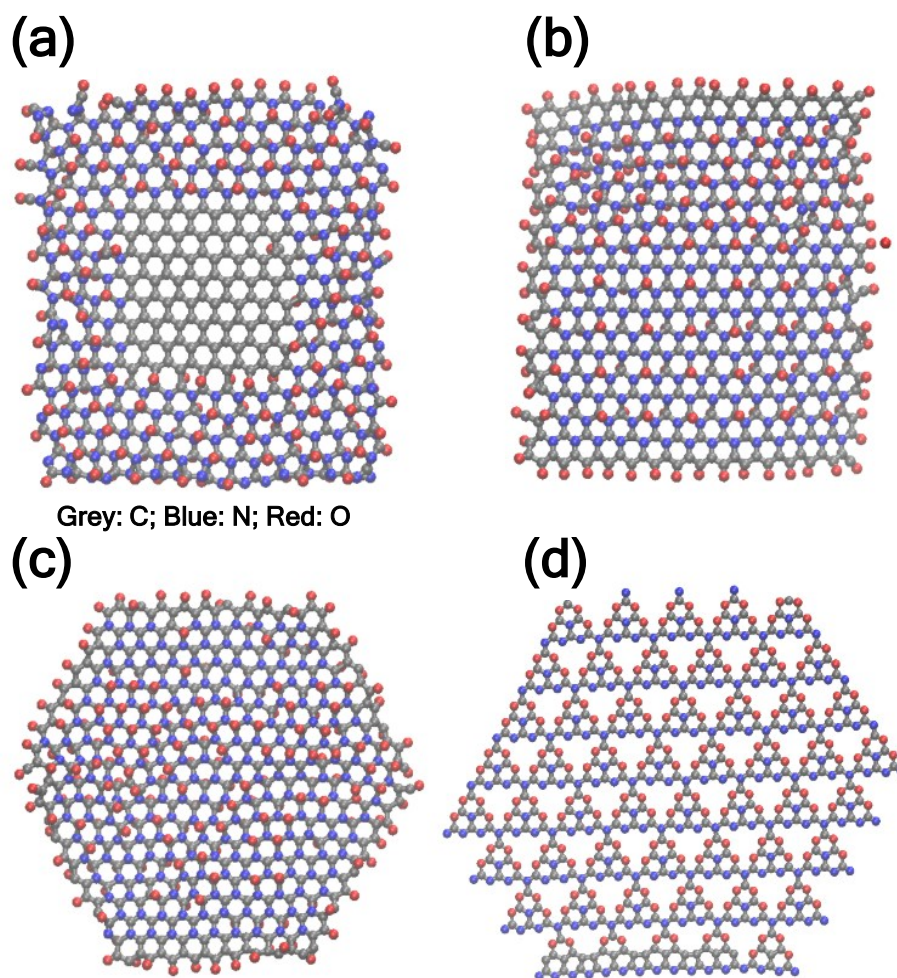Grey: C; Blue: N; Red: O

(c)

(d)

Figure S4.   Proposed atomic configurations of different 740-atom models (C/U: 1/2)

with the C: N: O atomic ratio of 325: 215: 200: (a,b,c) heavily N-doped

graphene with O adsorption and (d) heavily O-doped g-C_3N_4.

(a)

(b)

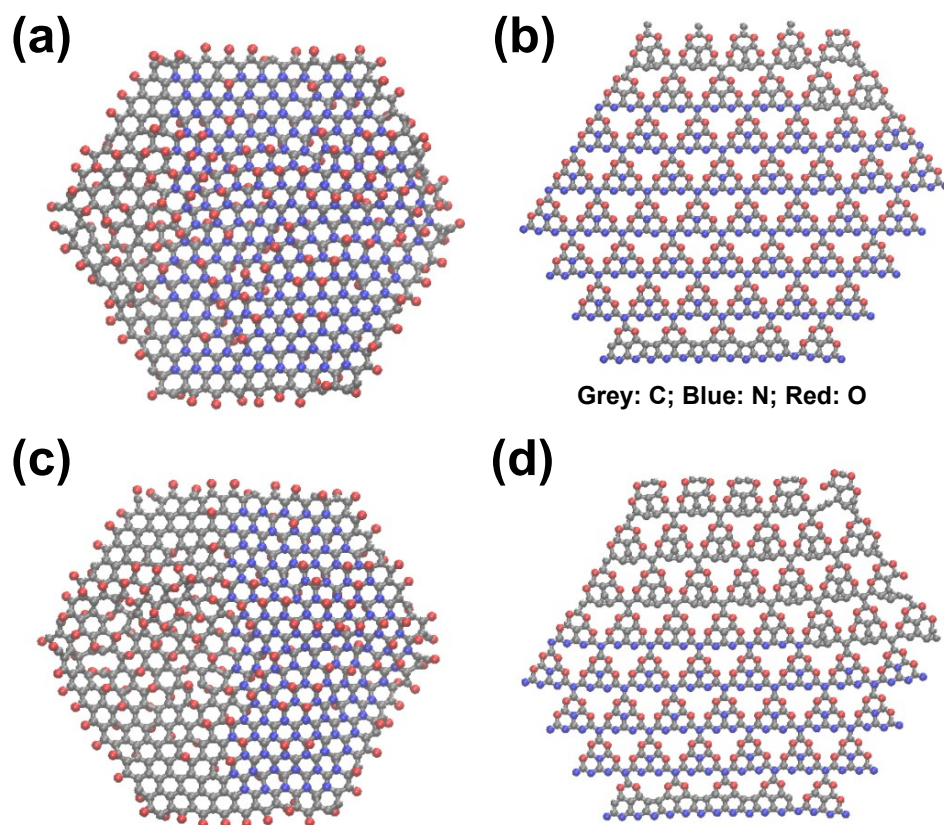**Grey: C; Blue: N; Red: O**

(c)

(d)

Figure S5.   Proposed atomic configurations of 740-atom models with different N/C

ratios: heavily N-doped graphene with O adsorption: (a) N/C= 24/49 and

(c) N/C= 15/53 and heavily O-doped g-C_3N_4: (b) N/C= 24/49 and (d)

N/C= 15/53.

Figure S6.   Photographs of N-doped CND samples prepared using the SPMA

method with C/U weight ratios of 3/1, 2/1, 1/1, 1/1.5, 1/2, and 1/3,

showing almost no sediments after six months.